

A Two-Stage Imaging Framework Combining CNN and Physics-Informed Neural Networks for Full-Inverse Tomography: A Case Study in Electrical Impedance Tomography (EIT)

Xuanxuan Yang^{1,2}, Yangming Zhang¹, Haofeng Chen^{1,2}, Gang Ma², Xiaojie Wang¹

Abstract—Physics-Informed Neural Networks (PINNs) are a machine learning technique for solving partial differential equations (PDEs) by incorporating PDEs as loss terms in neural networks and minimizing the loss function during training. Tomographic imaging, a method to reconstruct internal properties from external measurement data, is highly complex and ill-posed, making it an inverse problem. Recently, PINNs have shown significant potential in computational fluid dynamics (CFD) and have advantages in solving inverse problems. However, existing research has primarily focused on semi-inverse Electrical Impedance Tomography (EIT), where internal electric potentials are accessible. The practical full inverse EIT problem, where only boundary voltage measurements are available, remains challenging. To address this, we propose a two-stage hybrid learning framework combining Convolutional Neural Networks (CNNs) and PINNs to solve the full inverse EIT problem. This framework integrates data-driven and model-driven approaches, combines supervised and unsupervised learning, and decouples the forward and inverse problems within the PINN framework in EIT. Stage I: a U-Net constructs an end-to-end mapping from boundary voltage measurements to the internal potential distribution using supervised learning. Stage II: a Multilayer Perceptron (MLP)-based PINN takes the predicted internal potentials as input to solve for the conductivity distribution through unsupervised learning.

Index Terms—CNN, PINN, EIT, Inverse problem

I. INTRODUCTION

PHYSICS -Informed Neural Networks (PINNs) are a machine learning technique used to solve partial differential equations (PDEs). By incorporating the PDE as a loss term within the neural network, PINNs approximate the PDE solution by minimizing the loss function during training [1], [12].

Tomographic imaging is a method for reconstructing the internal properties of an object from external measurement

data. This process typically involves inferring internal structures from finite and potentially noisy external data, making it highly complex and ill-posed, and fundamentally belonging to the category of inverse problems [2].

Recently, PINNs have shown significant potential in computational fluid dynamics (CFD) and offer considerable advantages for solving inverse problems [3]. Consequently, there has been growing interest in exploring how PINNs can address tomographic imaging problems [6], [7]. Electrical Impedance Tomography (EIT) is a technique used to reconstruct internal conductivity distributions by injecting currents through boundary electrodes and performing boundary electrical measurements. Bar et al. and Pokkunuru et al. have investigated the application of PINNs for solving EIT problems [4], [5].

Bar et al. were the first to systematically solve the semi-inverse EIT problem using PINNs, achieving excellent results. They also applied this method to solve the full-inverse EIT problem. However, their work [4] demonstrated that they only validated relatively simple reconstruction shapes. Subsequently, Pokkunuru et al. introduced energy-based priors into PINNs to help the network converge more quickly and improve imaging accuracy and quality [5]. Nevertheless, their work was also limited to the semi-inverse problem, and their performance in full-inverse EIT was suboptimal. They stated: “we are able to recover σ accurately for simple anomalies like row one. However, when the phantom configuration becomes complex, the joint training fails.” Additionally, they attempted to reproduce Bar et al.’s work on full-inverse EIT but were unsuccessful. They claimed that since Bar et al.’s work was not open-sourced, they were unable to replicate the full-inverse EIT based on the details provided in the paper [4].

The semi-inverse problem involves reconstructing internal conductivity when the electric potential is accessible at any internal point. Although research into semi-inverse EIT has demonstrated some promising results with PINNs, practical applications typically involve the full inverse problem. In the full inverse problem, only boundary voltage measurements are available from electrodes, and the goal is to reconstruct the internal conductivity distribution from these measurements. This scenario presents a significantly greater challenge.

Given these challenges, the limitations of existing works are as follows:

- 1) Current successes with PINNs are mostly confined to

Xuanxuan Yang, Haofeng Chen are with the Institute of Intelligent Machines, Hefei Institute of Physical Science and University of Science and Technology of China, Hefei. Gang Ma is with the University of Science and Technology of China, Hefei, Anhui 230026, China (e-mail: magang93@ustc.edu.cn). Xiaojie Wang and Yangming Zhang are with the Institute of Intelligent Machines, Hefei Institute of Physical Science, Chinese Academy of Sciences, Hefei 230031, China (e-mail: xjwang@iamt.ac.cn; yz2898@columbia.edu).

This work was supported in part by the National Natural Science Foundation of China (Grant NO.62303436); in part by the Fundamental Research Funds for the Central Universities under Grant WK5290000004

Corresponding author: Gang Ma (e-mail: magang93@ustc.edu.cn) Xiaojie Wang (e-mail: xjwang@iamt.ac.cn)

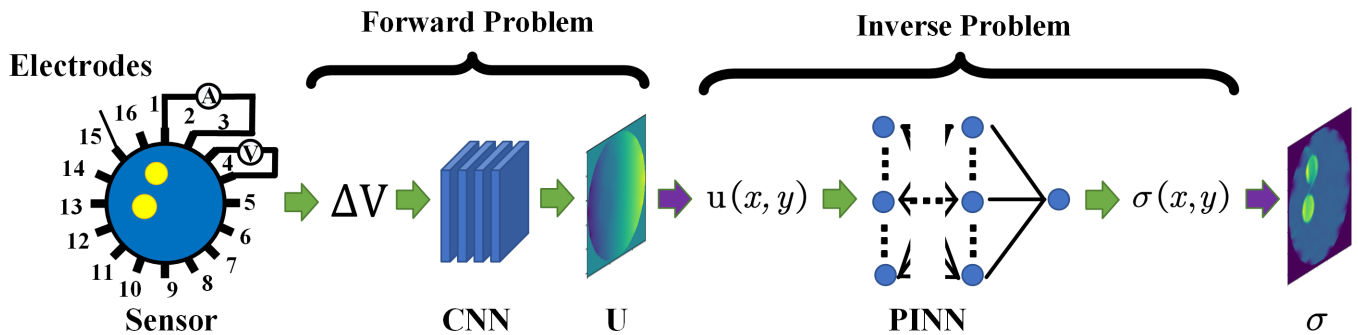


Fig. 1. The structural diagram of our proposed method.

the semi-inverse EIT problem, where they achieve good results under the ideal condition of accessing internal electric potentials. In contrast, the full inverse EIT problem, which relies solely on boundary voltage measurements, presents a greater challenge. Existing methods have struggled to perform effectively in this scenario [4], [5].

- 2) When applying PINNs to solve the full inverse EIT problem, if the measurement protocol necessitates changing the excitation electrodes to K different positions, it requires training K forward problem networks along with one inverse problem network. This significantly increases computational demands and time, posing a substantial challenge [4]–[6].
- 3) In the full inverse problem, the forward and inverse components are highly interdependent, or coupled, making iterative updates challenging. Achieving accurate performance often requires additional information, such as prior knowledge.

As can be seen, the forward problem plays a crucial role in solving full-inverse EIT. Considering the advantages of CNNs in image processing, we decided to use CNNs to directly predict the internal potential distribution, replacing PINNs for solving the forward problem. Convolutional Neural Networks (CNNs) are pivotal in image processing because of their capability to extract spatial features from images. They have achieved notable success in various tasks, including regression, segmentation, and detection. The generated tensor representing the internal potential is then subjected to matrix differentiation and fed into the PINN to solve the inverse problem. Consequently, we introduce a two-stage hybrid learning framework that combines CNN and PINN to address the full inverse EIT problem. This framework integrates data-driven and model-driven approaches, incorporates supervised and unsupervised learning, and decouples the forward and inverse problems within PINNs, making its application to the full inverse EIT feasible. The framework is detailed as follows:

Stage I: We employ a U-Net architecture to develop an end-to-end mapping from boundary voltage measurements to the internal potential distribution, generated under a fixed electrode excitation pattern. The goal is to accurately predict the internal potential distribution based on boundary voltage measurements. This stage involves a data-driven supervised

learning approach, where the model learns the spatial relationships between boundary measurements and internal potential distributions from an extensive dataset.

Stage II: We utilize a Multilayer Perceptron (MLP) with residual connections to build the PINN. The internal potential distribution $u(x, y)$ predicted from Stage I is input into the PINN to solve for the conductivity $\sigma(x, y)$ at each point. The loss function of the PINN is constrained by the PDEs relevant to EIT. This stage involves a model-driven unsupervised learning approach, wherein the conductivity distribution is inferred from the potential distribution.

The contributions of this paper are as follows:

- 1) **Proposing a Hybrid Learning Framework:** We propose a hybrid learning framework that integrates data-driven and model-driven approaches to solve the full inverse EIT problem. Compared to direct data-driven methods, which map boundary voltage measurements to internal conductivity distributions, our approach offers better interpretability [1]. The CNN extracts detailed spatial features, while the PINN ensures adherence to physical laws and boundary conditions.
- 2) **Efficient Forward Problem Solving:** By solving the forward problem using a data-driven approach, our method requires only a single training session on the relevant dataset to rapidly produce high-quality internal potential distributions. This efficient process establishes a robust foundation for solving the subsequent inverse problem and mitigates the time and computational resource demands associated with training multiple networks in PINNs for the full inverse EIT problem across varying conductivity distributions. [1], [4], [5].
- 3) **Decoupling the Forward and Inverse Problems:** By decoupling the forward and inverse problems, the CNN-predicted internal potential distribution serves as a favorable initial condition for PINN training. This reduces the sensitivity of PINNs to the hyperparameters of the forward problem and enhances training stability.
- 4) **Improving PINN Imaging Performance:** The integration of CNN and PINN in our method overcomes the poor imaging performance of PINNs in full inverse EIT, making them viable for practical tomographic applications. Furthermore, this combined approach can be extended to other inverse imaging problems, showcasing

its versatility.

II. METHOD

We utilize a 16-electrode EIT system with a unit circle radius of 1, with electrodes evenly distributed along the boundary. The system employs a complete electrode model (CEM) and a four-electrode measurement protocol. The collected voltage data are then input into our two-stage CNN and PINN hybrid framework for image reconstruction, as illustrated in Figure 1.

A. PDE in EIT

The partial differential equation governing EIT is given in Equation (1). The first term is an elliptic equation, where σ represents the conductivity and u denotes the electric potential. The second and third terms specify the boundary conditions, with n as the unit normal vector, g as the current density, and f as the measured potential. The fourth term describes the Neumann-to-Dirichlet (NtD) mapping.

$$\begin{cases} -\nabla \cdot \sigma \nabla u = 0 & \text{in } \Omega \\ \sigma \left(\frac{\partial u}{\partial n} \right) = g & \text{on } \partial\Omega \text{ Neumann BC} \\ u = f & \text{on } \partial\Omega \text{ Dirichlet BC} \\ \Lambda_\sigma : g \mapsto f \end{cases} \quad (1)$$

B. Forward problem networks

It is noteworthy that the real electric potential is not constant, which complicates the training of CNNs. Attempts to address this issue include using CNNs with attention mechanisms, residual networks, and auxiliary outputs of derivatives of electric potential. While these approaches can yield reasonably good results, they often produce noisy outputs, especially near boundaries due to the non-constant background. Such noisy results are not suitable for use in the subsequent inverse problem. Inspired by the success of the U-Net architecture in image segmentation, as demonstrated by Qin et al. [8], we constructed a U-Net to establish an end-to-end mapping from the boundary voltage measurements ΔV to the internal potential distribution U , generated under a fixed current excitation pattern. Additionally, drawing from related works [4], [5], [9], we set the current pattern to $g = \frac{1}{\sqrt{2\pi}} \sin(\omega k + \varphi)$. Given the finite number of electrodes, we set $\omega = \frac{2\pi}{16}$ and $\varphi = 0$, the resulting potential distribution is shown in Figure 2.

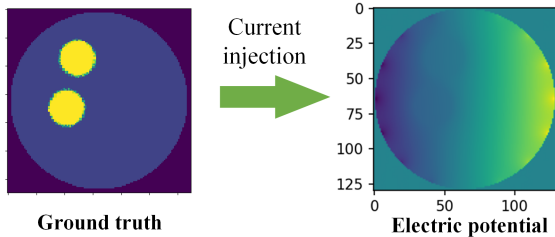


Fig. 2. Ground truth and potential distribution formed after current injection.

Next, we trained the network on a large dataset to predict the internal potential distribution generated under the excitation of the current pattern g given a set of boundary potential measurements. This network employs data-driven supervised learning to capture the spatial relationship between boundary voltage measurements and internal potential distributions from extensive data, as shown in Figure 3.

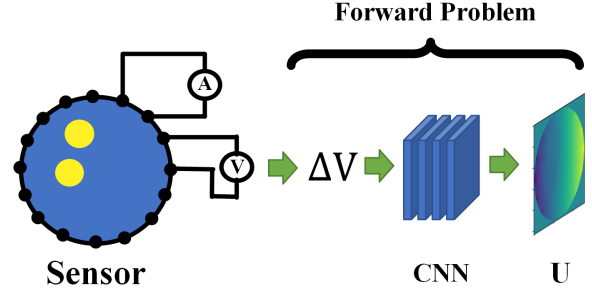


Fig. 3. Forward problem network architecture.

C. Inverse problem networks

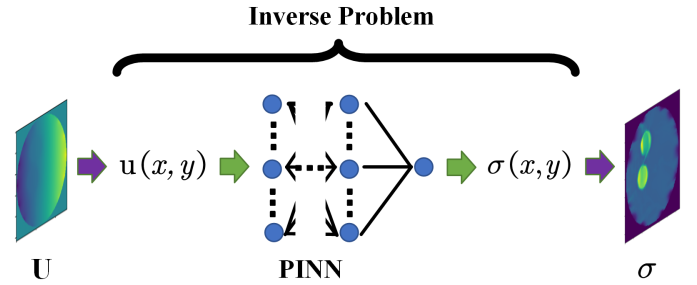


Fig. 4. Inverse problem network architecture.

Once we obtain the output U from the forward problem network, we can access the potential values $u(x, y)$ at any point within U . These potential values $u(x, y)$ can then be used to solve the inverse problem. Figure 4 illustrates the structure of the inverse problem network, which is a PINN. Inspired by the work of Wang et al. [10], the inverse problem network is a multilayer perceptron consisting of four hidden layers, each with 64 neurons and tanh activation functions, and incorporates residual connections at each layer to deepen the network and enhance its performance. The input to this network is the grid coordinates in the Cartesian space Ω , and the output is the conductivity value $\sigma(x, y)$ at each point.

$$\begin{aligned}
 \mathcal{L}_{inv-Net} = & \frac{\alpha}{\Omega} \sum_{d \in \{\Omega\}} (\nabla \cdot (\sigma_d \nabla u_d))^2 \\
 & + \frac{\beta}{M} \sum_{m \in \text{top}_M \mathcal{L}_{PDE}} |\nabla \cdot (\sigma_d \nabla u_d)| \\
 & + \frac{\gamma}{|\partial\Omega_b|} \sum_{b \in \partial\Omega_b} \left| \sigma_b \frac{\partial u_b}{\partial n_b} \right| + \frac{1}{|\partial\Omega|} \sum_{b \in \partial\Omega_b} |\sigma_b - \sigma_{\partial\Omega_b}^*| \\
 & + \frac{\tau}{|\Omega|} \sum_{d \in \Omega} \sqrt{\nabla_x \sigma_d + \nabla_y \sigma_d + \xi} \\
 & + \frac{\nu}{|\Omega \cup \partial\Omega|} \sum_{h \in \{\Omega \cup \partial\Omega\}} \max(0, 1 - \sigma_h) + \zeta \|w_\sigma\|^2
 \end{aligned} \tag{2}$$

According to the partial differential equations in Equation (1), we embed them into the loss function of the MLP, resulting in the loss function shown in Equation (2). The first term, derived from the elliptic equation, is the L_2 norm of the differential operator, which controls the potential u and conductivity σ . The second term is the L_∞ norm. Bar et al. demonstrated that the L_∞ norm provides a strong solution, ensuring that the equations are satisfied for isolated points [4]. The third and fourth terms are derived from the boundary conditions, where $\sigma_{\partial\Omega_b}^*$ is the known conductivity on the boundary points. The fifth term, inspired by the work of González et al. [11], is an isotropic total variation regularization term added to promote sparse boundaries in the predictions. The sixth term penalizes any conductivity prediction that is less than or equal to the conductivity of the vacuum, ensuring that the conductivity values cannot be less than 1. The final term is a regularization term to control the network parameters.

It is important to highlight that, in contrast to the approaches employed by Bar et al. [4] and Pokkunuru et al. [5], which utilize TensorFlow's `tf.gradients` function for the automatic computation of partial derivatives of the potential, our methodology deviates in a significant manner. Specifically, their methods involve auto-differentiating the forward network with respect to the x and y coordinates in the inverse problem, and similarly auto-differentiating the inverse network in the forward problem. This coupled relationship introduces complexities to the full inverse problem and can result in poor outcomes. In contrast, our approach involves the direct computation of partial derivatives of the potential matrix U with respect to the x and y coordinates using a matrix-based method. While this approach demonstrates superior performance, it should be noted that numerical differentiation via finite differences does not capture the same level of detail as the auto-differentiation of network functions in semi-inverse problem.

III. EXPERIMENTS AND RESULTS

A. Dataset

In the forward problem network, we selected 3000 data sets for training, allocating 10% for validation and another 10% for testing. The training dataset included configurations with a single circle, two circles, and a combination of a circle with a triangle. The background conductivity was fixed at 1, while the

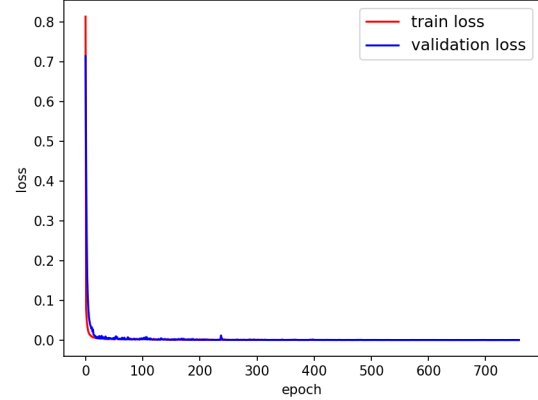


Fig. 5. The loss curves for the training and validation sets of the forward problem network

object conductivity ranged from 2 to 6, with object positions being randomly generated. We used the measured voltages differences, ΔV , as inputs and the corresponding internal potentials, generated under the current pattern g , as outputs for training. The training was performed using two GTX 3090 GPUs and took approximately 1.5 hours to complete around 800 epochs. The loss curves for both the training and validation sets are presented in Figure 5.

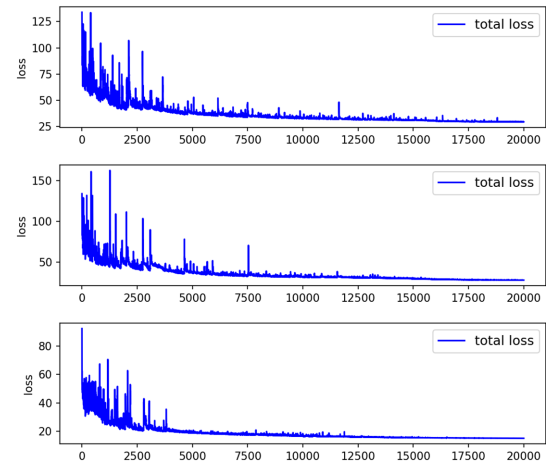


Fig. 6. The loss curves of the PINN.

B. Simulation experiments

To show imaging performance, we presented three test cases from the test set, each representing a special configuration. These test inputs were processed through both the forward problem network and the inverse problem network. The loss function of the inverse problem network is shown in Figure 6, with each training session taking 2 hours on two GTX 3090 GPUs. As demonstrated in Figure 7, our proposed method performs well even with multiple complex shapes, effectively addressing the full inverse EIT problem of reconstructing conductivity from boundary voltage measurements.

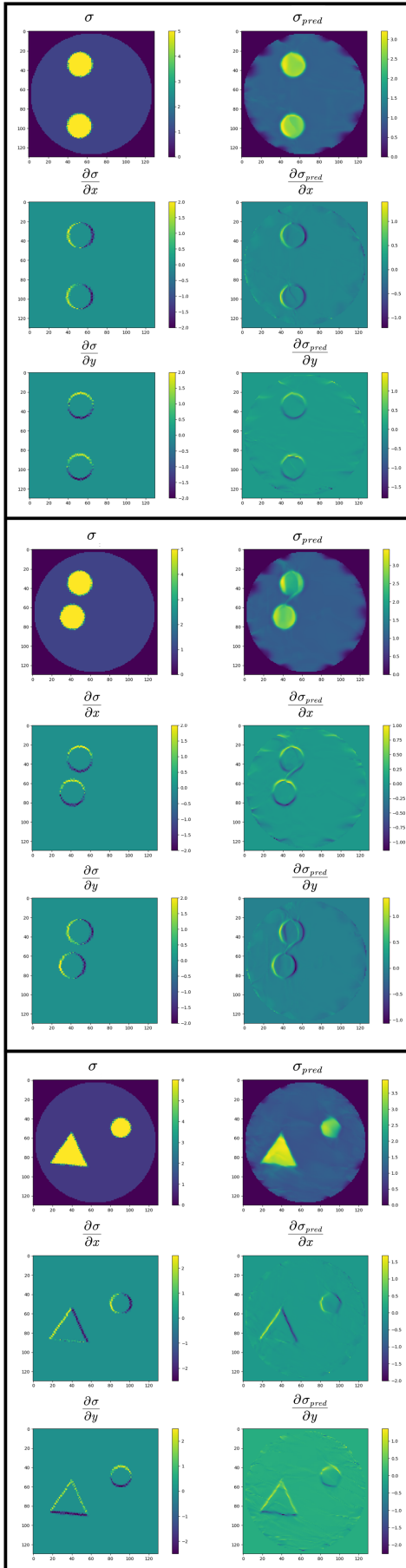


Fig. 7. Reconstructed images using our proposed method. The first column is the Ground truth, namely σ_g , and its partial derivatives with respect to x and y , and the second column is the σ and its partial derivatives with respect to x and y reconstructed by our method.

IV. CONCLUSION AND FUTURE WORK

In this study, we propose a two-stage method combining CNN and PINN to address the poor imaging performance of PINNs in full inverse tomography, using EIT as an example. This approach makes the application of PINNs in full inverse tomography feasible and can be extended to other inverse imaging problems. Future work will involve validating our method using real datasets and investigating the imaging performance in cases with non-smooth conductivity distributions of perturbed internal objects. Additionally, we aim to further optimize the forward problem network to predict internal potentials more quickly and accurately.

REFERENCES

- [1] S. Cuomo, V. S. Di Cola, F. Giampaolo, G. Rozza, M. Raissi, and F. Piccialli, "Scientific machine learning through physics-informed neural networks: Where we are and what's next," *Journal of Scientific Computing*, vol. 92, no. 3, p. 88, 2022.
- [2] J. Kaipio and E. Somersalo, *Statistical and computational inverse problems*. Springer Science & Business Media, 2006, vol. 160.
- [3] S. Cai, Z. Mao, Z. Wang, M. Yin, and G. E. Karniadakis, "Physics-informed neural networks (pinns) for fluid mechanics: A review," *Acta Mechanica Sinica*, vol. 37, no. 12, pp. 1727–1738, 2021.
- [4] L. Bar and N. Sochen, "Strong solutions for pde-based tomography by unsupervised learning," *SIAM Journal on Imaging Sciences*, vol. 14, no. 1, pp. 128–155, 2021.
- [5] A. Pokkunuru, P. Rooshenas, T. Strauss, A. Abhishek, and T. Khan, "Improved training of physics-informed neural networks using energy-based priors: a study on electrical impedance tomography," in *The Eleventh International Conference on Learning Representations*, 2023.
- [6] R. Guo, T. Huang, M. Li, H. Zhang, and Y. C. Eldar, "Physics-embedded machine learning for electromagnetic data imaging: Examining three types of data-driven imaging methods," *IEEE Signal Processing Magazine*, vol. 40, no. 2, pp. 18–31, 2023.
- [7] G. Ruan, Z. Wang, C. Liu, L. Xia, H. Wang, L. Qi, and W. Chen, "Magnetic resonance electrical properties tomography based on modified physics-informed neural network and multiconstraints," *IEEE Transactions on Medical Imaging*, 2024.
- [8] X. Qin, Z. Zhang, C. Huang, M. Dehghan, O. R. Zaiane, and M. Jagersand, "U2-net: Going deeper with nested u-structure for salient object detection," *Pattern recognition*, vol. 106, p. 107404, 2020.
- [9] S. Siltanen, J. Mueller, and D. Isaacson, "An implementation of the reconstruction algorithm of a nachman for the 2d inverse conductivity problem," *Inverse Problems*, vol. 16, no. 3, p. 681, 2000.
- [10] S. Wang, Y. Teng, and P. Perdikaris, "Understanding and mitigating gradient flow pathologies in physics-informed neural networks," *SIAM Journal on Scientific Computing*, vol. 43, no. 5, pp. A3055–A3081, 2021.
- [11] G. González, V. Kolehmainen, and A. Seppänen, "Isotropic and anisotropic total variation regularization in electrical impedance tomography," *Computers & Mathematics with Applications*, vol. 74, no. 3, pp. 564–576, 2017.
- [12] M. Raissi, P. Perdikaris, and G. E. Karniadakis, "Physics-informed neural networks: A deep learning framework for solving forward and inverse problems involving nonlinear partial differential equations," *Journal of Computational physics*, vol. 378, pp. 686–707, 2019.